ResearchGate

See discussions, stats, and author profiles for this publication at: https://www.researchgate.net/publication/323155240

A New Automatic Full-Waveform Regional Moment Tensor Inversion Algorithm and Its Applications in the Taiwa....

Article *in* Bulletin of the Seismological Society of America · February 2018

DOI: 10.1785/0120170231

CITATIONS
0

READS
46

4 authors, including:



Tai-Lin Tseng
National Taiwan University
45 PUBLICATIONS **570** CITATIONS

SEE PROFILE

Some of the authors of this publication are also working on these related projects:



Seismic Structures of the Caucasus and East Turkey View project

All content following this page was uploaded by Tai-Lin Tseng on 01 March 2018.

The user has requested enhancement of the downloaded file.

Bulletin of the Seismological Society of America, Vol. XX, No. XX, pp. –, – 2018, doi: 10.1785/0120170231

A New Automatic Full-Waveform Regional Moment Tensor Inversion Algorithm and Its Applications in the Taiwan Area

by Pei-Ru Jian, Tai-Lin Tseng, Wen-Tzong Liang, and Ping-Han Huang

Abstract A new algorithm has been developed in this study that can automatically determine regional moment tensor (MT) and its centroid depth with real-time waveforms; it can do this within 2–4 min of an earthquake notice issued by the Central Weather Bureau (CWB). The program selects 3–7 BATS (Broadband Array in Taiwan for Seismology) stations based on three different strategies: best azimuthal distribution, highest signal-to-noise ratio, and shortest distances. The program then inverts MT solutions in parallel with various settings that include Moho depth of velocity models, frequency bands, and isotropic constraints. The optimal solution is determined via a search for the best waveform fit with an acceptable non-double-couple component that comes from the results of combinations of these inversion settings. Our new rapid MT report system greatly reduces the need for computational resources and avoids human judgments. By applying this full-scanning approach on BATS (named AutoBATS), we redetermine the MTs for over 3000 regional earthquakes that took place between 1996 and 2016, the goal being to provide the most up-to-date possible MT catalog for the Taiwan area. Overall, the AutoBATS MTs are consistent with the Global Centroid Moment Tensors, with a mean difference in the Kagan angle of $22.0° \pm 16.6°$ and M_w of -0.08 ± 0.10. Those focal mechanisms better illuminate the tectonic structures, which is a result of the significantly improved resolving ability for shallow (< 10 km) and deep (> 140 km) earthquakes. With the new regional MT catalog, we refine the relationship between moment and local magnitudes: $M_w = 0.87M_L + 0.23$ for the Taiwan region.

Introduction

Timely determination of source parameters for large regional earthquakes is crucial for government agencies to be able to properly and quickly respond to cases of serious seismic hazards. Reliable estimates of the seismic moment and focal mechanism are particularly important because these two parameters are directly related to the extent and severity of the seismic damage caused by the earthquakes. For long-term evaluation of the seismic hazard of seismically active regions, a robust regional moment tensor (MT) catalog is the most fundamental information for the conduction of advanced studies in areas such as regional tectonics, strain–stress monitoring of the lithosphere, and strong-motion simulation for hazard evaluations.

For moderate-to-large earthquakes with M_w above ~5.5 worldwide, MT solutions are available freely from multiple agencies/organizations, including the Global Centroid Moment Tensor (CMT) project (Ekström *et al.*, 2012), the U.S. Geological Survey (USGS; Sipkin, 1986), GEOFON (Bormann, 2012), and GEOSCOPE (Vallée *et al.*, 2011). In theory, both the CMT and point-source parameters (centroid position and origin time) are determined by inverting very long-period seismic waveforms recorded at teleseismic distances (Dziewonski *et al.*, 1981). Over the past two decades, regional MT inversion has also become a routine process to release MT or CMT local catalogs for small-to-moderate earthquakes because regional seismic networks have built up in many seismically active areas (Dreger and Helmberger, 1993; Sileny *et al.*, 1996; Kao, Jian, *et al.*, 1998; Fukuyama and Dreger, 2000; Braunmiller *et al.*, 2002; Kubo *et al.*, 2002; Pondrelli *et al.*, 2002; Stich *et al.*, 2003; Bernardi *et al.*, 2004; Ito *et al.*, 2006; Cambaz and Mutlu, 2016). With increasingly dense regional networks developing worldwide, near-real-time automatic MT inversion systems are becoming possible, due to the large improvements in data transmission and computational capability that have been developed in the last decade (e.g., Bernardi *et al.*, 2004; Rueda and Mezcua, 2005; Ito *et al.*, 2006; Nakano *et al.*, 2008; Scognamiglio *et al.*, 2009; Lee *et al.*, 2011). On a regional scale, genuine CMT solutions can be inverted based on local long-period waveforms, with the centroid position often obtained by grid-search approaches (e.g., Ito *et al.*, 2006; Lee *et al.*, 2014).

Taiwan, an extremely seismically active area in the western Pacific, was one of the first countries to have a regional MT reporting system. Kao, Jian, *et al.* (1998) established the MT inversion algorithm using long-period waveforms that were recorded by the local network Broadband Array in Taiwan for Seismology (BATS; see Data and Resources); this was operating under the Institute of Earth Sciences (IES) of Academia Sinica, Taiwan. Since 1995, the Data Management Center (DMC) of IES has routinely inverted and published over 2000 MT solutions for regional earthquakes with M_L above 4.0. The MTs released by IES BATS (so-called BATS CMT) have been widely adopted by research communities for further investigations in the Taiwan area on earthquake rupture characteristics (e.g., Huang *et al.*, 2008; Lee *et al.*, 2008), seismotectonic studies (e.g., Kao, Shen, and Ma, 1998; Kao and Jian, 1999; Kao and Chen, 2000; Kao *et al.*, 2000; Lallemand *et al.*, 2001; Angelier *et al.*, 2009; Chen *et al.*, 2009; Huang *et al.*, 2017), seismic moment magnitudes, and seismic hazard evaluations (e.g., Chen *et al.*, 2008).

To achieve timely estimates of MTs for Taiwan earthquakes, IES BATS currently performs MT inversion with a set of fixed parameters; it does this after receiving alarms issued by the Central Weather Bureau (CWB) of Taiwan. However, data selection and quality examination on inversion results are still performed manually. Usually, the MT reports can be provided within a few hours. From a different perspective, Lee *et al.* (2014) developed a real-time MT system that reports the centroid hypocenter location with a 10-km spatial resolution, as well as the corresponding MT, within 2 min; it does this by calculating MTs of a continuous data stream that are recurrently recorded by a fixed subset of BATS stations. The drawback of this state-of-the-art system is the requirement of significant computational resources to approach a truly real-time solution that is independent of the CWB report.

No matter which frameworks are chosen, it is unquestionable that the reliability of the MT solution requires the inversion itself to be performed with suitable parameters and settings. In particular, lateral changes in velocity structure are apparent in Taiwan (e.g., Rau and Wu, 1995; Huang *et al.*, 2014), and a fixed 1D model cannot be perfect for each event analyzed. The MT solutions may be improved by adjusting 1D velocity models for each event–station pair, selecting alternative stations, and trying different frequency bands for each station. In the past, for BATS MT, further fine-tuning was also manually processed (Kao *et al.*, 2002; Liang *et al.*, 2004). However, this traditional approach is too tedious and inefficient to satisfy current demand, leading to the desire for a compromise. In addition, it is important to explore how large the variances can be if the solutions are inverted with different parameters or settings.

In Taiwan, reporting MT solutions while satisfying both fast and reliable obligations is a great challenge, due to strong heterogeneity in velocity structures, possible mislocation of off-island earthquakes, and unavoidable long-period background noises for those stations located close to shore or on small islands. In this study, we develop a new automatic approach that will help achieve the goal of retrieving highly reliable regional MT solutions in near-real time for small-to-moderate earthquakes in Taiwan. We are not attempting to fully determine the centroid hypocenters. Instead, we take advantage of the overall efficiently and precisely determined epicenter origins from CWB. Therefore, only the centroid depth and MT of the events are constrained in our MT report. To reduce the manual efforts on searching suitable inversion settings for each earthquake, we determine the final MT solution among the inversion results by systematically exploring various key settings or parameters; these include different frequency bands, station-selection strategies, and 1D velocity models. Then, we can demonstrate the variability of the solutions and discuss which factors are more influential on the MTs for each event. Finally, we provide 20 years of well-determined focal mechanisms for the Taiwan region that exhibit details of tectonic features.

Moment Tensor Inversion and Regional Waveform Data

Linear MT inversion is based upon the representation theorems in which the observed displacement waveforms are the combined effects of the earthquake source and Green's functions (Aki and Richards, 1980). In principle, Green's functions contain propagation effects in a layered Earth's structure from earthquake to station; in contrast, an MT is a matrix of six independent elements and gives the equivalent radiation of faulting on a point source. In the case of zero-volume change, the third isotropic element is compensated for by the sum of the other two on the diagonal of the matrix (Jost and Herrmann, 1989), yielding five independent variables to solve. With a properly derived velocity model and quality waveforms, the MT can be directly inverted by minimizing the overall differences between the observed and simulated three-component waveforms in a least-squares sense (Stump and Johnson, 1977). The fault parameters are then derived from the double-couple (DC) component of the MT.

In the current CMT inversion algorithm of BATS, Kao, Jian, *et al.* (1998) used a reflectivity-based method of Yao and Harkrider (1983) to calculate Green's functions. In this study, we employ the frequency–wavenumber integration technique as an alternative that is capable of calculating both static and dynamic surface displacement (Zhu and Rivera, 2002). For the goodness of waveform fitting in the inversion, we principally follow the definition of a cross-correlated similarity-sensitive misfit function (introduced by Mellman *et al.*, 1975; Kao, Jian, *et al.*, 1998), which emphasizes the coherence between the observed and synthetic waveforms more than the absolute amplitudes (Wallace *et al.*, 1981). To further account for the differences in relative amplitude, we adopt the misfit equation for each component as follows: $E=1-\frac{\min(f_i(t)_{\max},g_i(t)_{\max})}{\max(f_i(t)_{\max},g_i(t)_{\max})}\frac{\int f_i(t)g_i(t)dt}{\sqrt{\int f_i(t)^2dt\int g_i(t)^2dt}}$, in which $f_i(t)$ and $g_i(t)$ are observed and synthetic waveforms in displacement,

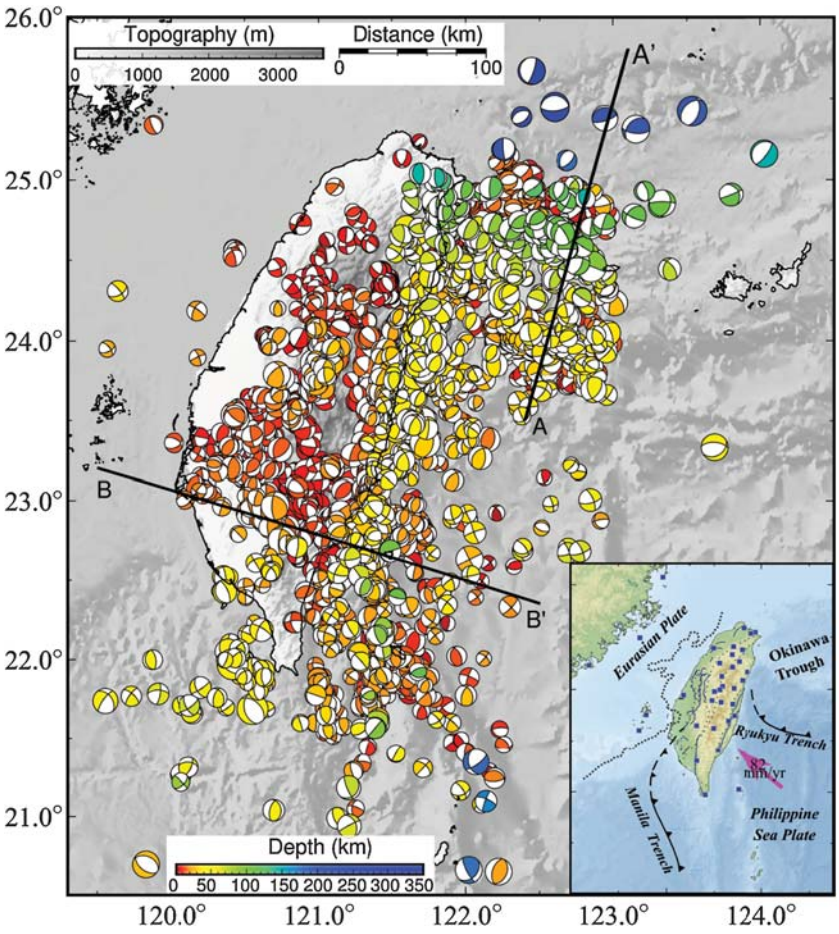


Figure 1. Map showing the results of AutoBATS (full-scanning approach on Broadband Array in Taiwan for Seismology [BATS]) moment tensor (MT) inversion for earthquakes that took place between May 1996 and April 2016. The focal mechanism plot colors represent the centroid depth determined by MT inversion. The size of projected focal sphere is scaled with the moment magnitude. (Inset) The tectonic setting in the Taiwan area. The pink thick arrow indicates the direction of the converging Philippine Sea plate relative to the Eurasian plate. BATS broadband stations are denoted by blue squares (excluding stations in the South China Sea). The dotted line delineates the 2000 m isopach of Cenozoic sediments.

respectively; $f_i(t)_{\max}$ and $g_i(t)_{\max}$ are the maximum amplitude of observation and synthetic waveforms, respectively (Kao and Jian, 1999; Huang *et al.*, 2017).

In this study, all broadband waveforms come from BATS, a local network that currently consists of a total of 36 broadband stations in the Taiwan area (Fig. 1, inset) that have been providing high-quality continuous seismic data since 1996 (Institute of Earth Sciences, Academia Sinica, Taiwan, 1996). The initial information about each earthquake, including epicenter, focal depth, and origin time, is taken from CWB. To reduce the effects of mislocation errors on inversion results, we only use well-determined hypocenters of earthquakes that have been manually verified by CWB with the quality-checked data. The centroid depth of the MT solution, along with the MT inversion, is estimated using a grid-search approach; this is done as it is in many CMT studies (Dreger and Helmberger, 1993; Zhu and Helmberger, 1996), as well as the previous BATS inversion (Kao, Jian, *et al.*, 1998). Here, we perform MT inversion at a 1 km interval for a depth range of ±12 km, with respect to the initial focal depth; the centroid depth is determined from the smallest misfit among the 25 solutions.

Although the MT inversion itself is a linearized problem through Green's functions and seismic displacement waveforms, nonuniqueness or large variances of inversion results are common because of nonlinear effects/bias from the different 1D velocity model assumptions for Green's functions, the frequency band used for data processing, and the method of selecting stations. Therefore, our approach is to retrieve stable MT solutions by systematically scanning the solutions from all combinations of station-choosing strategies, varied velocity models, and different frequency bands. The scanning parameters and setting criteria are introduced in the next section.

Automatic Determination of the Optimal MT Solution with Thoroughly Scanned Parameters

To efficiently achieve stable and reliable results for MT inversion, the first important and necessary step is to make sure that manual data selection is avoided before the inversion. In this study, we only consider stations whose average signal-to-noise ratios (SNRs) of three-component waveforms are greater than 2.0 in the desired frequency band (0.01–0.09 Hz). We take 150 s time windows before and after the *P* arrival to estimate the spectra and calculate average point-by-point SNR with five-point moving time-window smoothing. We exclude stations with epicentral distances smaller than 30 km to reduce the mislocation effect. Because many studies typically use three or more three-component broadband stations for regional MT inversion (Dreger and Helmberger, 1993; Zhu and Helmberger, 1996; Kubo *et al.*, 2002; Pondrelli *et al.*, 2002; Rueda and Mezcua, 2005; Clinton *et al.*, 2006; Ristau, 2008), we selected a minimum of three to a maximum of seven SNR-qualified stations to start the inversion based on three different criteria: (1) the best azimuthal coverage, (2) the highest SNR, and (3) the shortest epicentral distances. For earthquakes inside a homogeneous network, the most logical and easiest approach for criterion (1) is to divide stations evenly into eight half-quadrants according to azimuth and pick at least one SNR-qualified station in each sector. Unfortunately, this simple method is not appropriate

for Taiwan, due to restricted azimuthal coverage in most cases; the majority of earthquakes occur near the coast and eastern offshore region. To accommodate this natural condition, we retain the stations at the minimum and maximum azimuth, and use these two azimuths as boundaries to divide the remaining stations into three even sectors. Then, we pick one to three stations randomly in each sector so that criterion (1) is fulfilled. For criteria (2) and (3), stations are chosen solely according to their mean SNR and epicentral distances.

It is normally expected that better azimuthal coverage improves reliability of MT solutions. The problem of selecting stations solely based on azimuthal coverage in the Taiwan area is that the selected stations near the coast or on small islands are occasionally contaminated by long-period ambient noises, even though the average SNR might be slightly better than threshold value. Criteria (2) and (3) not only provide other possible choices of stations, but the consistencies among resulting solutions can further ensure the MT solutions are insignificantly biased by those stations with notable noises near the shore or at far distances. The quality (SNR) of regional waveforms is usually site dependent and unrelated to epicentral distances; therefore, the three different criteria are complementary.

Once stations are selected, we perform the inversions with different parameter settings. To accommodate the velocity variations in the Taiwan region and to improve the stability of inversion with the longest possible periods, we apply three different frequency bands and four velocity models for all selected stations in the inversions. For each earthquake, three consecutive passbands are applied from the following five standard frequency ranges: 0.01–0.04 Hz (25–100 s), 0.02–0.06 Hz (16–50 s), 0.03–0.08 Hz (12–33 s), 0.04–0.09 Hz (10–25 s), and 0.05–0.15 Hz (7–20 s). The choice depends on the local magnitude reported by CWB. For earthquakes with a local magnitude above 5, within 3.5–5, and below 3.5, the lowest corner frequency starts from 0.01, 0.02, and 0.03 Hz, respectively.

For the velocity models, it is unrealistic to create a high-resolution 1D velocity model that reflects all the path effects for each event–station pair because the seismic waves usually travel through distinct structures in Taiwan (especially along the east–west direction). Considering that the waveforms for MT inversion have been filtered for relatively long periods, we start with a simple three-layer model averaged from a 3D tomography model of Taiwan (Rau and Wu, 1995) as a reference. This model, whose Moho depth is set at 40 km, has been used for 20 years by the current BATS MT inversion, and simulations in waveforms are reasonable in terms of fitness (Kao, Jian, *et al.*, 1998; Kao and Jian, 1999, 2001; Kao and Chen, 2000; Kao *et al.*, 2002; Liang *et al.*, 2004). Then, we further consider the effect of regional variations of Moho depths from 20 to 50 km under different geologic units that were revealed by receiver function and tomography studies (Wang *et al.*, 2010; Kuo-Chen *et al.*, 2012; Huang *et al.*, 2014). Because deeper than 20 km into the ground, the dominant periods used are more sensitive to structure than they are in the shallow crust within 10 km of the surface (Dahlen and Tromp, 1998), we create a series of velocity models by changing the Moho at five different depths ranging from 25 to 45 km with intervals of 5 km. Each candidate potentially represents the average/pseudo structure under the paths covered by the event. Moho depths between 30 and 45 km are used for inland earthquakes, whereas a shallower range from 25 to 40 km is considered for offshore cases. After carefully examining the inversion results, we confirmed that trying different Moho depth models can effectively reduce misfit and the compensated linear vector dipole (CLVD) component. Following Dreger (2003), we allow Green's functions to shift by ± 2 s for each station to lower the misfit, due to the possible mislocation and the flaws in the velocity model. For fast MT inversion, the Green's functions of each 1D model were precalculated and stored in the databases with a 1-km grid size in distance and focal depth.

For a more realistic simulation of synthetic waveforms, we assigned 0.5, 1.0, and 2.0 s as durations of the source time function for earthquakes with magnitudes in the following categories: smaller than 4, between 4 and 6, and above 6, respectively. Because events associated with volcanic activities have been reported in the Okinawa trough in northeast Taiwan (Lin *et al.*, 2007), our newly developed MT inversion method includes three different isotropic conditions: free-constrained, limited ($\leq 10\%$), and zero isotropic components. For the free-constrained or zero isotropic component, we simply invert either six or five independent elements of the MT. For limited isotropic constrained inversion, we compose a weighting vector inside the kernel matrix, in which the sum of three isotropic elements equals 0, as shown in the following form: $d = \begin{pmatrix} G \\ w\ w\ w\ 0\ 0\ 0 \end{pmatrix} \begin{pmatrix} m_{11}\ m_{22}\ m_{33}\ \cdots \end{pmatrix}^T$. The inversion is performed iteratively with an initial weighting factor (w) 1; it is then adjusted by increments of 1 until the isotropic component of the MT is reduced to 10% or lower.

The AutoBATS MT inversion starts with auto picking of the first *P* arrivals for each station (Allen, 1978). The system then performs all inversion processes concurrently with the different combinations of settings/parameters previously mentioned, using the GNU parallel tool (Tange, 2011). Among those inversion results, the one with the minimum misfit and applicable non-double-couple (non-DC) component is reported as the final/preferred MT solution (see Table 1 for classifications). Generally, we expect both the CLVD and isotropic components of the tensor to be low for small- to moderate-size tectonic earthquakes associated with shear faulting and relatively uncomplicated ruptures. According to Kagan (2002), an additional non-DC component can be introduced, due to the data contamination of background noises, an oversimplified velocity model, or the mislocation of earthquakes; therefore, we set up rigorous criteria for non-DC. Only solutions with an isotropic component $\leq 20\%$, CLVD $\leq 30\%$, and non-DC $\leq 40\%$ are accepted for reporting. For each resultant MT solution, we assign a quality factor according to the waveform misfit

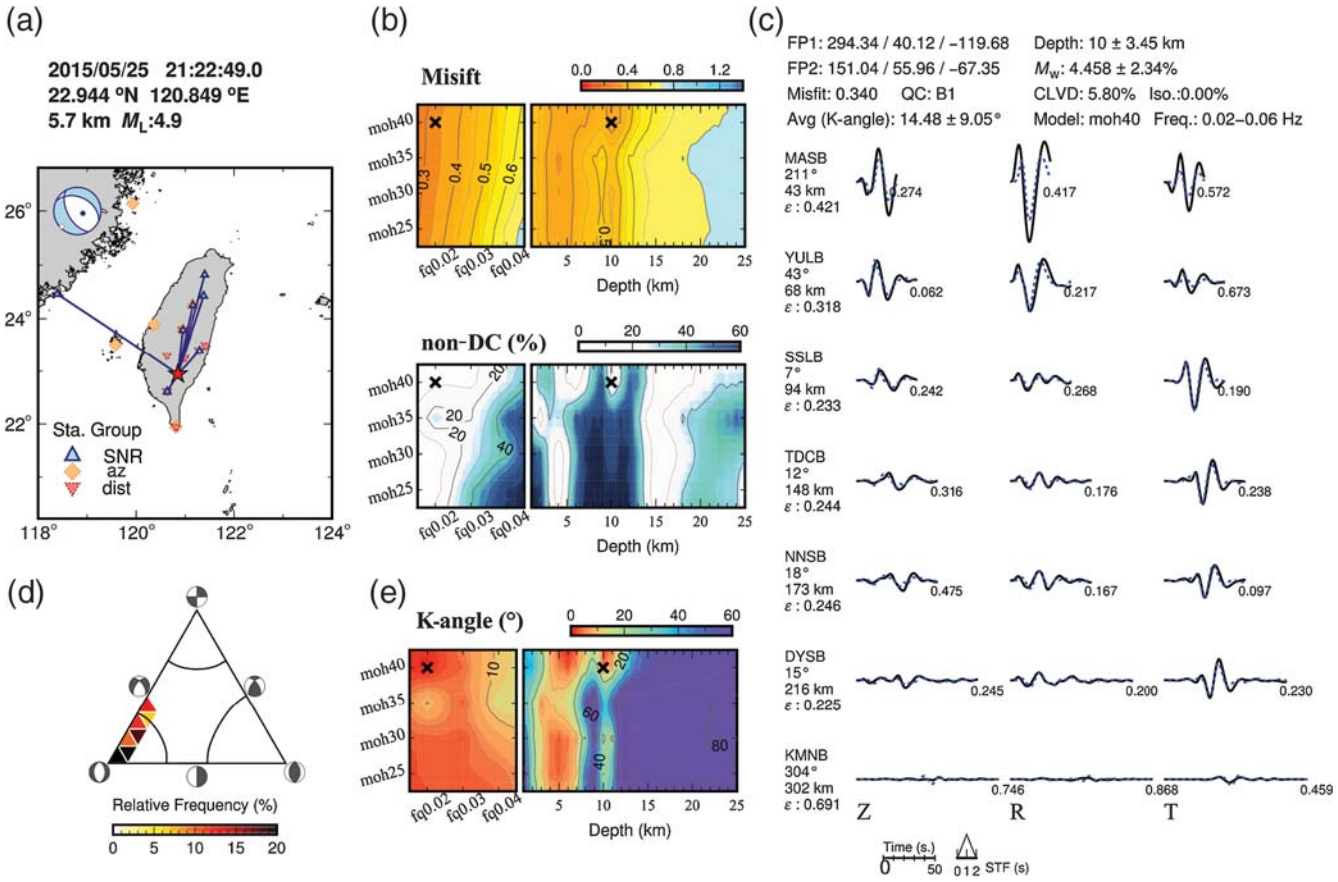


Figure 2. Results of MT inversion for the earthquake that occurred on 25 May 2015 (M_L 4.9) in the central range. (a) Map showing earthquake epicenter (red star) and distribution of three station groups (dist, shortest distance; az, best azimuthal coverage; SNR, highest signal-to-noise ratio) considered in the inversion scanning scheme. The stations used for the final/best solution are highlighted with bolded outlines. The final MT solution is shown in the upper left corner. The original time, epicenter, focal depth, and local magnitude reported by Central Weather Bureau (CWB) are listed at the top. (b) Contour images of (top) misfit and (bottom) non-double-couple (non-DC) for 4 varied Moho depth velocity models, 3 different frequency bands, and 25 scanned focal depths. The crosses mark the best suited combination of parameters used to produce the final MT solution. (c) The fitness between observations (solid black lines) and synthetic waveforms (blue dashed lines) corresponding to the best solution. For each station, the name of stations, azimuth angles, epicentral distances, and the average misfits of three-component waveforms are indicated on the left. The number beside each seismogram is the individual misfit. CLVD, compensated linear vector dipole. (d) The distribution of appearance (in percentage) on the focal mechanism triangular diagram from all inversion results with different inversion settings. The symbols are colored with the appearance frequency. (e) Contour images of the Kagan angles (K-angle) measured from the 3D rotation angle between the final focal mechanism and all other MT solutions. The explanations of axes and symbols are the same as in (b).

and non-DC component (Table 1). Although the MT solutions with limited non-DC components were reported, the AutoBATS parameter-scanning algorithm is capable of searching for the nontectonic seismic events if the non-DC criterion is removed.

Table 1
Quality Classifications of the Misfit and Non-Double-Couple (non-DC) Component in the Released AutoBATS Moment Tensor (MT) Catalog

Misfit	Category	Non-DC Component (%)	Class
< 0.3	A	< 10	1
0.3–0.5	B	10–20	2
0.5–0.7	C	20–30	3
> 0.7*	D	> 30*	4

AutoBATS, full-scanning approach on Broadband Array in Taiwan for Seismology (BATS).

*Program rejects solutions with non-DC components larger than 40% or misfits greater than 0.75.

In this study, we applied the procedure of AutoBATS MT inversion to determine a total of 3058 solutions for earthquakes that took place between May 1996 and April 2016 in the Taiwan region and had an M_L greater than 3.5 (Fig. 1). Figures 2 and 3 demonstrate how well the focal mechanisms are constrained by the AutoBATS inversion for a shallow earthquake (M_L 4.9) inland and another intermediate-depth event (M_L 6.7) offshore, respectively. In each event, the best solution of focal mechanism and the corresponding stations used are highlighted (Figs. 2a, and 3a). Inversion results from different combined settings (such as Moho depth of models, frequency bands, and centroid depths) are directly compared in terms of their misfits and non-DC components. For the 25 May 2015 inland earthquake, the distribution of misfit

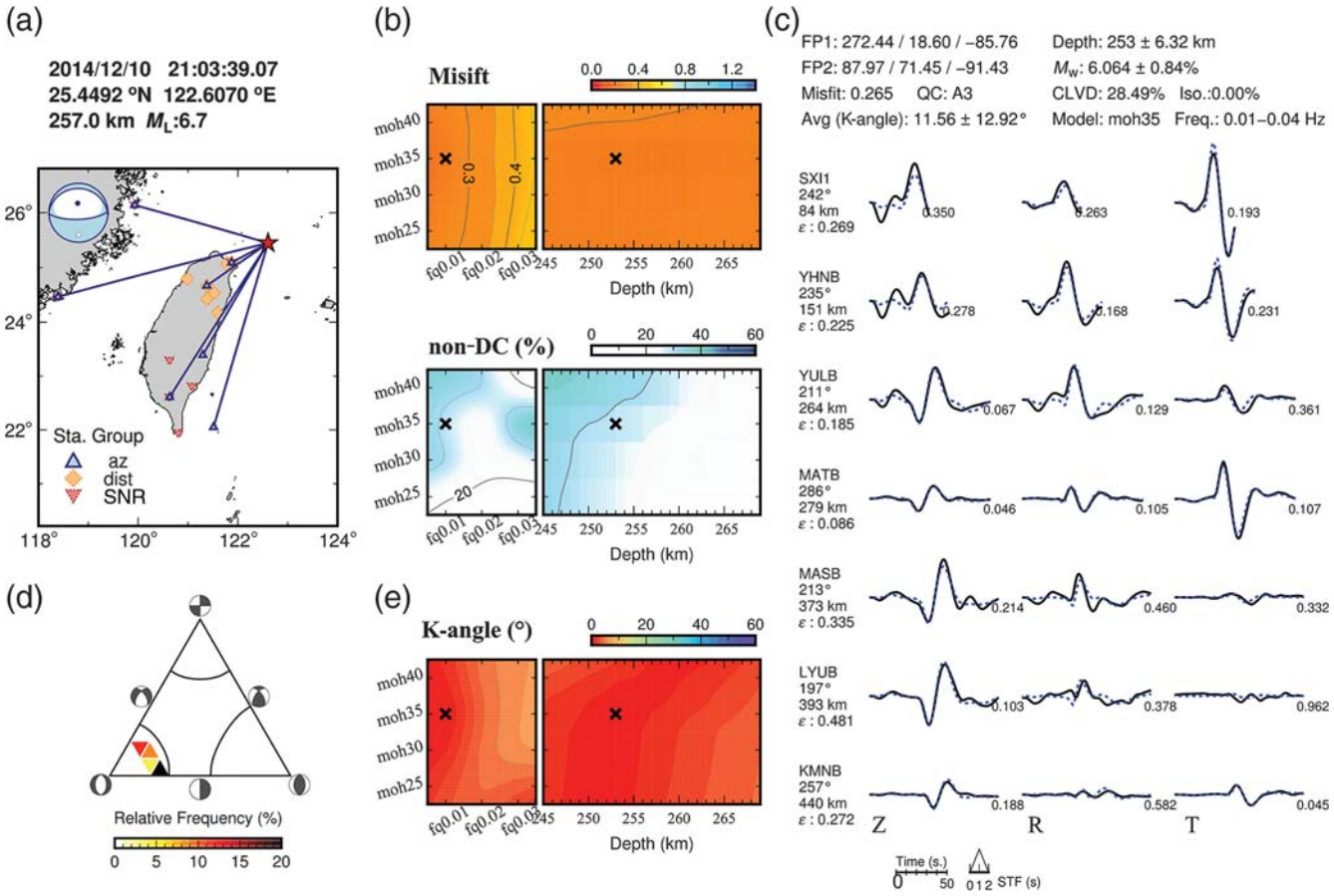


Figure 3. Results of MT inversion of the intermediate-depth earthquake that occurred on 10 December 2014 (M_L 6.7) beneath the Ryukyu subduction zone. The layout is the same as in Figure 2.

and non-DC contours shows that filtering at a lower frequency band (0.02–0.06 Hz) and a model with a deeper Moho of 40 km yields the smallest misfit for this normal-faulting event with a centroid depth of 10 km (Fig. 2b). Most inverted tensors are close to pure normal faulting, as indicated by the triangle diagram of focal mechanism (Fig. 2d). The triangle diagram, developed by Frohlich (2001), is an effective way to demonstrate the fault-type partitioning and the frequency distribution of the focal mechanisms from the inversion results of all tested parameters. Figure 2e goes further and provides us with the distribution of the Kagan angles (Kagan, 2003), which will hereafter be referred to as the K-angle; this is the smallest 3D rotation angle measured between the best focal mechanism and other solutions. It can be shown that the differences between solutions are more sensitive to the focal depths than the frequency band or velocity model for this earthquake. The overall small misfit is also evident by the excellent agreements between the observed and synthetic waveforms calculated from the final solutions (Fig. 2c). The uncertainties of moment magnitude, focal depth, and CLVD component are assessed through the standard deviation (st.dev.) from all scanned resultant inversions. This example reveals that the non-DC component of the low misfit (< 0.4) solutions can vary significantly with Moho depth and frequency band (Fig. 2b). The variability of solutions also confirms the necessity of scanning various settings while performing a regional MT inversion.

Figure 3 shows the result of an intermediate-depth earthquake that occurred in the offshore area of northeast Taiwan on 10 December 2014. This earthquake was excluded in the previous BATS MT catalog because the original depth reported by CWB exceeds the BATS MT calculation range. Our new AutoBATS inversion can provide more constraints to the subduction zone earthquakes. Unlike the shallow event shown in Figure 2, the misfit, non-DC component, and K-angle of this mid-focus offshore earthquake are relatively insensitive to velocity model, frequency bands, and focal depth; this results in highly coherent focal mechanisms and less varied misfits (Fig. 3). Because this earthquake is large in magnitude (M_w 6.0), filtering at a lower frequency band produces a smaller misfit than otherwise would be expected (Fig. 3d). Although the azimuthal coverage of stations is restricted to one quadrant, our MT solution and centroid depth estimation are both highly consistent with the solution from Global CMT (Ekström *et al.*, 2012). For intermediate-depth earthquakes, the centroid depths are sometimes more difficult to resolve within our ±12 km scanning depth range because the misfit values are comparably small (Fig. 3b). In addition to a reliable

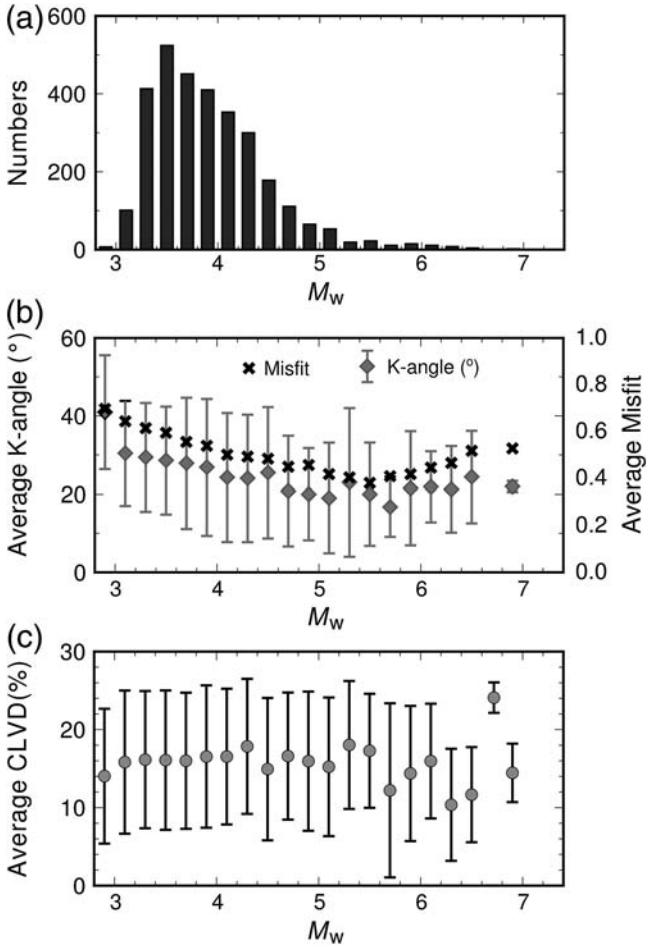


Figure 4. (a) Histogram showing the numbers of earthquakes with respect to M_w (bin size = 0.2). (b) The relationships between average misfit/K-angle and M_w, based on all AutoBATS MT solutions. (c) The relationship between average CLVD and M_w. The error bars in both (b) and (c) correspond to a standard deviation.

initial location from the CWB catalog, it is always recommended to consider other independent constraints, such as the depth phases *pP* and *sP* observed at teleseismic distance, to further confirm the actual depth of the event.

The AutoBATS MT inversion scheme shows superior capability for determining focal mechanisms. This study successfully resolved 3058 MTs (about 56%) out of 5500 CWB-reported earthquakes with acceptable data quality. Moreover, among these MT solutions, 87% have misfit values smaller than 0.7 (above category C in quality), and 99% have non-DC below 30% (above class 4). Some resolved earthquakes are as small as M_w 3.0 (Fig. 4a). With the new AutoBATS catalog, we can further investigate whether the mean misfit, value of the CLVD component, and consistency of MT solutions (as described by the K-angle) are related to the earthquake magnitudes. Figure 4b shows that as the moment magnitude increases from 3.5 to 5.6, the average misfit decreases from 0.7 to 0.4. This can be simply explained by the higher data quality against background noise for larger events. For earthquakes with $M_w \geq 5.6$, the average misfit increases again. This phenomenon may relate to the complexity of earthquake rupture, which often involves source directivity and multiple fault segments with different slip vectors, particularly in the cases of large events. Waveforms excited by complex source ruptures cannot be well simulated by a single focal mechanism, and so larger misfits may exist. In this case, the results of MT inversion represent the overall effect of averaged rupture for the earthquakes. Like the features observed for misfit, the mean K-angle shows almost exactly the same trend; the values first decrease and then increase with magnitude (Fig. 4b). The similarity between mean misfit and K-angle suggests that the stability and consistency of MT inversion results are mainly affected by the waveform quality for small–medium earthquakes and rupture complexity for larger earthquakes.

Contrarily, the mean CLVD appears to be a constant-independent of the magnitude of events (see Fig. 4c). This phenomenon agrees with Kagan (2002), who concluded that CLVDs are usually caused by artificial effects, except for well-examined events. As already demonstrated in Figure 2b, the CLVD component of a shallow earthquake is easily affected by different inversion settings. For Taiwan earthquakes, we believe that the strong heterogeneity in tectonic structures and the long-period ambient noises for some stations are mostly responsible for the observed high CLVDs. The lower limit of the average K-angle or CLVD (defined by mean value minus a st.dev.) for each M_w bin is reflective of the overall consistent MTs or small CLVDs among all scanning settings that is characteristic of those earthquakes. On the other hand, the upper bound (mean value plus a st.dev.) reveals that the MT solutions are tremendously affected by different inversion settings. Again, the deviations (error bars) of the average K-angle and CLVD highlight the importance and necessity of probing the best solutions through comprehensive scanning on different inversion settings or parameters.

Comparisons and Discussions

Consistency between Global CMT and AutoBATS MT Solutions

It is essential to evaluate the stability of our AutoBATS MT results by comparing the solutions with those in the Global CMT catalog, which is considered the most complete and reliable CMT database for earthquakes with magnitudes above ~5.5 that have taken place since 1976 (Dziewonski *et al.*, 1981; Ekström *et al.*, 2012). We focus on the consistencies in MTs and centroid depths. Because the CMT inversion results can be significantly influenced by mislocation and focal depth, we consider the focal mechanisms only for the matched events (based on original time) that are reasonably close to each other. First, we evaluate how close is close enough for an event pair. The histogram in Figure 5a indicates that the differences in epicenter locations for most matched event pairs are smaller than 20 km, and the mean difference measured from all 200 pairs is 15.7 ± 12.9 km. Figure 5b

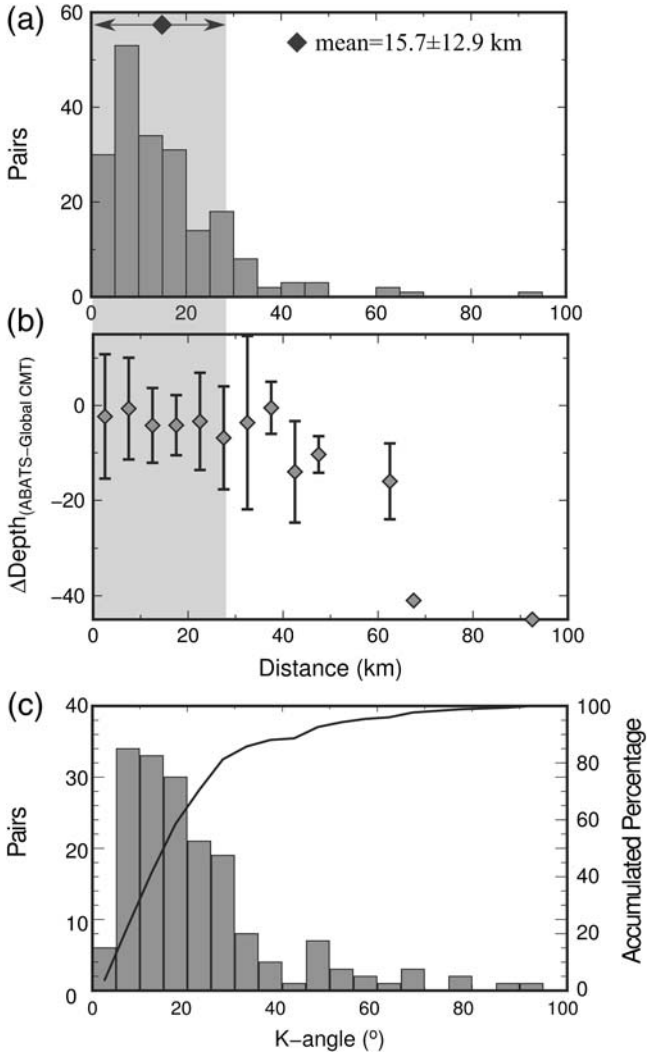


Figure 5. Diagram illustrating the consistency between AutoBATS MT and Global Centroid Moment Tensor (CMT). (a) Numbers of matched event pairs and (b) average depth differences between matched pairs in AutoBATS MT and Global CMT catalogs with respect to the epicenter difference (bin size for distance is 5 km). Only the earthquakes within the cutoff epicentral distance (shaded area) are included in the MT comparison between Global CMT and AutoBATS catalogs shown in (c) and Figure 6. (c) The K-angle distribution for 176 event pairs in the final comparison.

further confirms that the centroid depths reported in AutoBATS and Global CMT are consistent with each other when their locations are close. However, the discrepancy in centroid depth ($\Delta\text{depth} = d_{\text{ABATS}} - d_{\text{GlobalCMT}}$) and their standard deviation tends to grow much larger when the epicenter locations differ by 30+ km. Therefore, we use 28.6 km (the mean distance plus one st.dev.) as the distance cutoff and compare the MT solutions for pairs with an epicenter difference shorter than this value. There are 176 event pairs satisfying this criterion, and their MT solutions are further compared (Figs. 5c and 6).

Overall, more than 80% of the matched event pairs have K-angles smaller than 30° with a mean of 22.0° ± 16.6° (Fig. 5c). The remarkable consistencies between AutoBATS and Global CMT are also evidenced by the small difference in centroid depth (Δdepth) of -2.8 ± 9.8 km. We further investigate their correlations with magnitude, depth, and geographic locations (Fig. 6). Apparently, most matched events are located in the ocean (Fig. 6a). The relationship between the K-angle and M_w demonstrates that larger earthquakes tend to have smaller differences in MT solutions, meaning more consistency between the two catalogs (Fig. 6b). The largest discrepancy in K-angle appears in the group with the smallest magnitude 4.4–4.6 (only six events). This is probably because teleseismic long-period records suffer more from the background noise for small earthquakes ($M_w \leq 4.6$) in Global CMT. The negative mean $\Delta\text{depth}(d_{\text{ABATS}} - d_{\text{GlobalCMT}})$ indicates that Global CMT tends to obtain deeper centroid depths when compared with AutoBATS solutions (Fig. 6c). The MT solutions can differ quite a bit (K-angle > 60°) when focal depths are poorly constrained (as is the case in Fig. 2), especially for those located farther offshore from Taiwan and with poorer azimuthal coverage (Fig. 6a,c). Except for the two events with focal depth differences exceeding 40 km, all other pairs from the two catalogs seem reasonably consistent for the focal mechanisms (i.e., smaller K-angles), particularly when Δdepth is negative (Fig. 6c).

Statistically speaking, our AutoBATS MT solutions for $M_w > 4.6$ earthquakes agree well with the Global CMT reports. The comparison results reveal several key reasons for differences and help identify advantages/disadvantages of AutoBATS. First, the azimuthal coverage of local BATS is quite limited for earthquakes in the ocean far offshore from Taiwan. Under this condition, Global CMT can perform better than AutoBATS, as long as the earthquakes are large enough for quality recordings at global seismic distances; this is because events that could potentially come with large errors in hypocenters have been excluded in the comparison. For earthquakes in inland Taiwan, the regional MT inversion of AutoBATS can provide greater opportunities to solve reliable MT solutions. Second, the velocity models used are different. The global velocity model used by Global CMT for all earthquakes worldwide is more suitable for fitting very long-period teleseismic waveforms (above 40 s) of large earthquakes, which may not be ideal for the accurate determination of focal depth for moderate earthquakes (Dziewonski *et al.*, 1981; Ekström *et al.*, 2012). For regional MT inversion, although the heterogeneity of the velocity structure under the array is challenging, the accuracy can be improved in our AutoBATS MT inversion by exploring different Moho depths of the velocity models and grid-searching suitable focal depths. Third, different frequency bands used for Global CMT and AutoBATS MT inversions are likely to yield systematic variance of focal mechanisms and centroid depths between the two catalogs. The appropriate frequency range for regional CMT inversion is around 10–50 s, but longer periods (above 45 s) are more typical for global studies. Kagan (2003) studied the difference between two global CMT catalogs (Global CMT and NEIC MT), and the resulting average K-angle was 25.3° ± 16.5°;

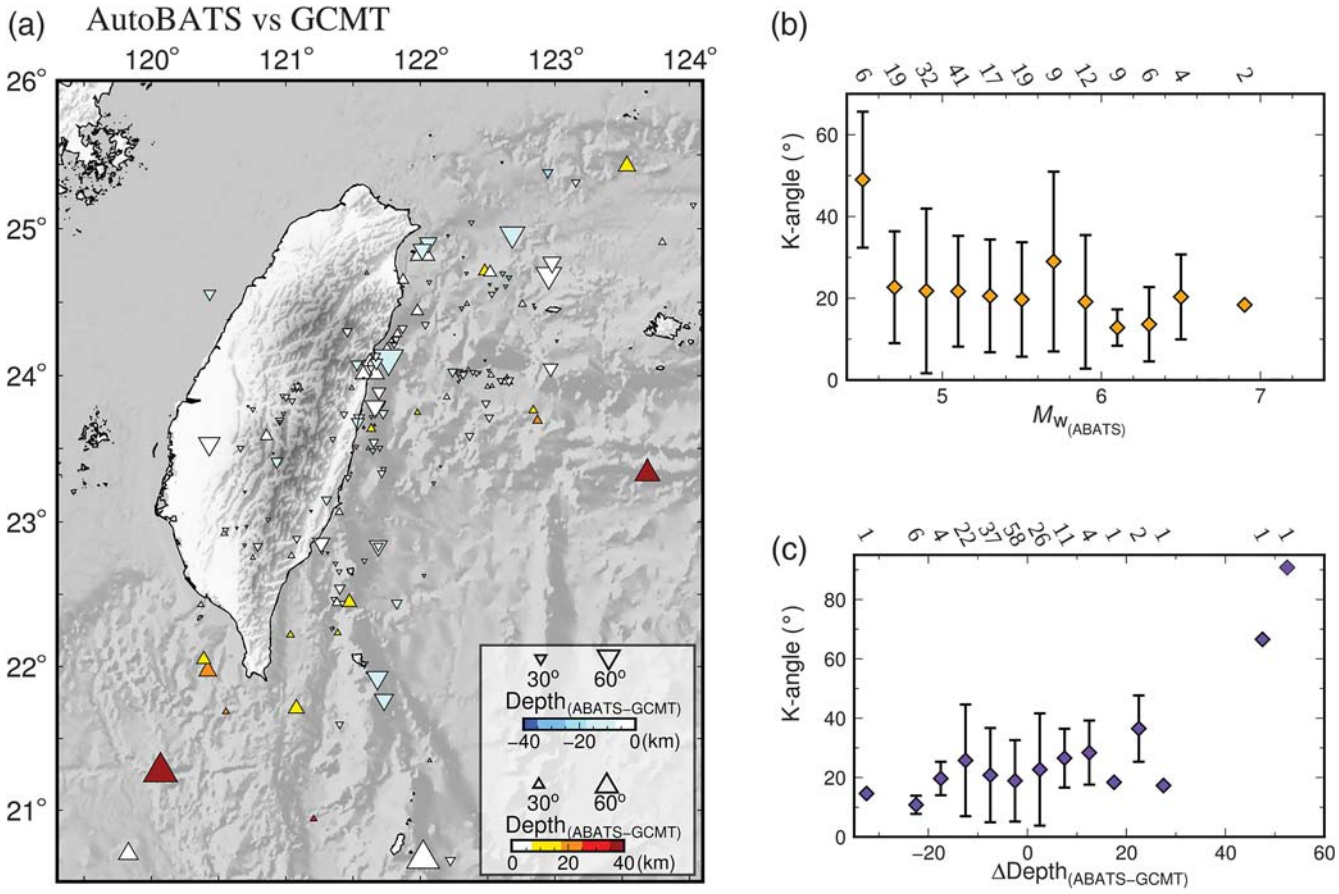


Figure 6. Comparisons of the focal mechanism and centroid depth between AutoBATS (denoted ABATS in this figure) and Global CMT (denoted as GCMT) catalogs. (a) Map showing the differences in MT (measured by K-angle) and depth for all matched event pairs. Locations of symbols (triangles) are plotted according to reported epicenters by CWB. The size of symbols is scaled with the K-angle, and the color represents the centroid depth of AutoBATS relative to Global CMT (i.e., AutoBATS minus Global CMT). Triangles and inverted triangles represent event pairs with AutoBATS depths that are deeper and shallower than Global CMT's estimates, respectively. (b) The relationship between average K-angle and magnitude (bin size of magnitude = 0.2). (c) The relationship between average K-angle and $\Delta\text{Depth}_{(\text{ABATS}-\text{GCMT})}$ (bin size of depth = 5 km). The numbers of earthquakes in each bin are denoted at the top of each panel.

this was based on 1385 earthquakes with magnitudes greater than or equal to 6. This value is comparable with our mean difference for Taiwan (22.0° ± 16.6°), suggesting that the AutoBATS MT inversion scheme developed in this study has the ability to retrieve reliable MT results. When more event pairs are accumulated, we can perform similar analyses on CLVD and focal depth, as in Kagan (2003); this will help us to fully evaluate the effects of mislocations on the focal mechanisms determined from AutoBATS and Global CMT catalogs.

Comparisons between the Original BATS and New AutoBATS MT Solutions

There are 1176 event pairs that have been matched from the original BATS and the new AutoBATS MT catalogs. Because both catalogs are based on the same local seismic network data and similar simple three-layer velocity models, we expect the results to be more consistent than those from AutoBATS versus Global CMT. To our surprise, the mean K-angle (31.4° ± 22.3°) was considerably higher, although the mean $\Delta\text{depth}_{\text{ABATS}-\text{BATS}}$ (−1.8 ± 8.7 km) was reduced by 1 km with a comparable st.dev. relative to $\Delta\text{depth}_{\text{ABATS}-\text{GlobalCMT}}$. Large discrepancies in K-angles were found in northeast and southeast offshore areas, where the Ryukyu subduction zone tends to have a relatively deeper centroid depth for AutoBATS, but the opposite situation exists beneath the Luzon Arc (Fig. 7a). Some earthquakes in the Central Mountain Range also showed prominent K-angle differences. Unlike those events offshore, their $\Delta\text{depth}_{\text{ABATS}-\text{BATS}}$ were generally small and slightly negative (BATS deeper than AutoBATS). We believe that this is because focal depths shallower than 10 km are not resolvable, and a fixed velocity model was used in the previous BATS inversion. Figure 7b shows that the K-angle basically remains constant (around 30°) until M_w 5.0; then, it gradually decreases to 20° as the magnitude increases to a M_w value around 6. The exceptions occur at extreme magnitudes; it is probably a result of higher noise levels for small events and complex ruptures for large events. Another important finding involves the strong dependency of the mean K-angle

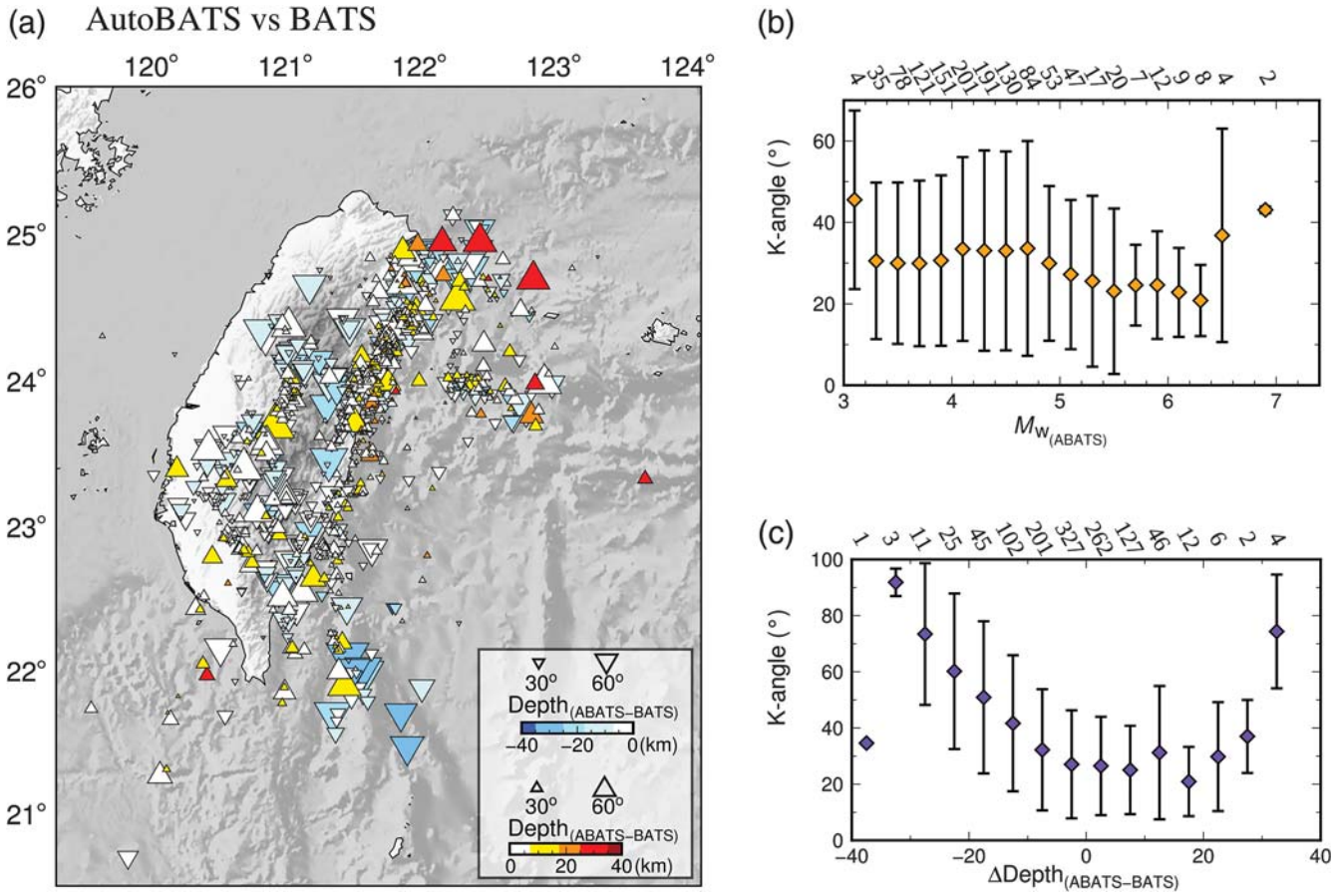


Figure 7. Comparisons of the focal mechanism and centroid depth between AutoBATS (denoted ABATS) and BATS catalogs. (a) Map showing the differences in MT (measured by K-angle) and depth for all matched event pairs. Sizes and colors of symbols are the same as in Figure 6a. (b) The relationship between average K-angle and magnitude. (c) The relationship between average K-angle and $\Delta\text{Depth}_{(\text{ABATS}-\text{BATS})}$. The numbers of earthquakes in each bin are denoted at the top of each panel.

on the differences of centroid depth measured from BATS and AutoBATS MT catalogs. Figure 7c reveals a positive correlation between the mean K-angle and the depth differences. This pattern is appreciably different from Figure 6c for the comparisons between AutoBATS and Global CMT, which proves again the strong dependency of MTs on focal depth for regional MT inversion. Overall, the centroid depths from the AutoBATS MT catalog are more consistent with the relocated focal depth in the CWB catalog, as indicated by the mean and st.dev. of differential depth ($|\Delta\text{depth}_{(\text{ABATS}-\text{CWB})}| = 2.6 \pm 6.9$ vs. $|\Delta\text{depth}_{(\text{BATS}-\text{CWB})}| = 4.4 \pm 8.4$).

We notice that there is no event with a centroid depth shallower than 10 km in the original BATS catalogs. After careful inspections and one-to-one comparisons on several shallow earthquakes, we believe the limited resolution on depth in the current BATS catalog is caused by insufficient resolution of the Green's function calculation algorithm or the inversion process itself. In contrast, the new AutoBATS MT inversion is able to resolve centroid depth in the shallow crust without problems. In addition to the improvements on the focal depths, our new AutoBATS MT solutions are also relatively consistent with Global CMT. This is clearly supported by larger $\text{K-angle}_{\text{BATS}-\text{GlobalCMT}}$ ($27.4° \pm 18.9°$ from 204 event pairs), compared with $\text{K-angle}_{\text{ABATS}-\text{GlobalCMT}}$ ($22.0° \pm 16.6°$ from 176 pairs).

The BATS data center used to release the so-called final MT solutions (FCMTs of BATS), which were obtained by fine-tuning the inversion settings manually after relocated earthquake bulletins of CWB were available (Kao and Jian, 1999; Kao *et al.*, 2001). Because of the restriction on human resources, starting from November 2006, BATS only reports quick MT solutions (QCMTs) based on CWB's preliminary epicenters, a fixed frequency band (0.03–0.08 Hz), and a three-layer velocity model with Moho depth at 40 km. We divide BATS CMTs into two subsets, FCMTs and QCMTs, and compare them separately with AutoBATS MT solutions. By excluding those shallow events that might have the depth problems mentioned in the previous paragraph, we find that the mean $\text{K-angle}_{\text{FCMT}-\text{ABATS}}$ ($33.8° \pm 25.0°$) is apparently larger than $\text{K-angle}_{\text{QCMT}-\text{ABATS}}$ ($24.4° \pm 15.6°$). Even though time-consuming efforts had been made to manually adjust the MT inversion parameters or settings, the greater deviation of FCMTs solutions from AutoBATS implies that the quality of inversion results strongly relies on the experi-

ences of operators who produced FCMTs, as well as how many settings or parameters have been tried thoroughly for the MT inversion. It also supports the assertion that a comprehensive scanning is necessary and an effective way to produce a reliable MT catalog.

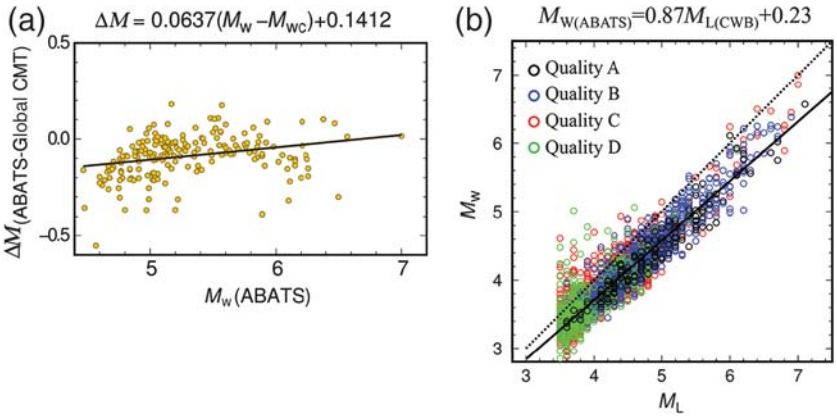


Figure 8. (a) Relationship of M_w differences between AutoBATS (denoted ABATS) and Global CMT with respect to $M_{w(ABATS)}$. M_{wc} in the regression relationship is the minimum M_w in the AutoBATS catalog. (b) The relationship between $M_{L(CWB)}$ and $M_{w(ABATS)}$. The symbols are colored according to the inversion quality factor. The dashed line marks the 1-to-1 ratio. Regression is performed for earthquakes above quality C.

Moment Magnitude and Local Magnitude Relationship for Taiwan

It has been noted that the moment magnitude is usually underestimated for earthquakes determined from regional seismic networks when compared to those obtained from global studies (Chen *et al.*, 2008; Gasperini *et al.*, 2012). Gasperini *et al.* (2012) found the mean difference of estimated M_w to be negligibly small (only about 0.027) for earthquakes in the European–Mediterranean area. For the Taiwan region, Chen *et al.* (2008) compared the M_w of BATS MT/CMT catalog with Global CMT for 79 event pairs and found a significantly large mean offset of about 0.3. They proposed that the underestimation of M_w by BATS was caused by insufficient low-frequency signals used in the regional MT inversion. This issue does not exist in our new AutoBATS MTs because the mean offset of M_w between the AutoBATS MT and Global CMT catalogs is very small (-0.08 ± 0.10). Accordingly, the reasoning suggested by Chen *et al.* (2008) can be ruled out. Compared with our AutoBATS MTs, the M_w from BATS is indeed smaller by 0.15 ± 0.18 on average, similar to the value recently reported by another regional MT study in Taiwan (Lee *et al.*, 2014).

We further investigate whether the M_w differences between AutoBATS and Global CMT have any relationship to the sizes of earthquakes. In Figure 8a, regression from all event pairs shows a straight line with positive slope, defined by the equation $\Delta m = a_1(m - m_c) + a_0$. In this equation, m is the M_w from the AutoBATS; m_c is the minimum M_w of the compared event pairs from AutoBATS; Δm is the ABATS-Global CMT magnitude difference; and a_1 and a_0 are the slope and bias terms. When the regression coefficients a_0 and a_1 are close to zero, the differences in magnitude are likely caused by random errors rather than systematic errors (Kagan, 2003). This is indeed the case ($a_1 = -0.017$ and $a_0 = 0.002$) for the M_w comparison between Global CMT and USGS-MT catalogs, whereas a systematic bias ($a_0 = 0.280$) and dependence of magnitude ($a_1 = 0.141$) between M_w (from Global CMT) and M_b (from Preliminary Determination of Epicenter) are predictable (Kagan, 2003). Compared with our AutoBATS to Global CMT catalogs, the minor bias term ($a_0 = 0.14$), along with the small mean M_w offset (-0.080 ± 0.10), shows that the underestimations on M_w in the AutoBATS catalog are negligible. The small slope ($a_1 = 0.063$) also indicates that the difference in M_w between AutoBATS and Global CMT is not significantly related to magnitude.

Hanks and Boore (1984) used earthquakes in California to demonstrate that, in principle, the M_L is equivalent to M_w for the magnitude range from 3 to 5. However, deviation from the 1:1 relation between M_w and M_L is commonly observed in other regions (Hanks and Boore, 1984; Deichmann, 2006). If the relation can be described by $M_w = aM_L + b$, the results usually vary widely depending on the geographical region (frequency-dependent attenuation), focal depth (Ristau, 2009), magnitude range, formulations of the empirical distance correction used for calculating M_L (e.g., Shin, 1993; Ristau *et al.*, 2003), and the algorithm for deriving M_w (Bethmann *et al.*, 2011). Over- or underestimating M_L can seriously influence the calculation of magnitude recurrence relations (b-values), which are related to seismic hazard. With many reliably estimated M_w from the AutoBATS MT catalog, we determine a new linear regression relation of seismic moment and local magnitude for the Taiwan area. As Figure 8b shows, M_w and M_L are correlated linearly for a large range of magnitudes from M_L 3.5 to 7. Because data with quality level D are dominant in small events and relatively scattered, we use qualities A–C (total of 2667 pairs) to estimate the relationship: $M_{w(ABATS)} = 0.87M_{L(CWB)} + 0.23$ (or equivalently $M_{L(CWB)} = 1.01M_{w(ABATS)} + 0.28$). The result is comparable with $M_{L(CWB)} = 1.05M_w + 0.25$, which was estimated using 3 years of real-time CMTs (Lee *et al.*, 2014). Basically, an earthquake reported with M_L 7.0 would correspond to a much smaller M_w of only about 6.3. The size of moment and local magnitudes are more comparable for small events. Based on the properties of scaling relations modeled in Switzerland (Edwards *et al.*, 2010), we speculate that the increase of M_w–M_L differences with respect to magnitude is controlled by attenuation, and the continuation of linearity to magnitude 6+ implies stress drop at the order of 10 MPa

or more. The high stress drop is consistent with the reported values for major earthquakes in Taiwan (Huang *et al.*, 2001; Yen and Ma, 2011). Our data set includes both collision and subduction zones covering inland and offshore Taiwan. Regional variation is expected. To understand the first-order changes in property, we attempt to calculate two separate regressions for 2396 shallower (depth ≤ 40 km) and 271 deeper (depth > 40 km) events with a quality above C. Then, we find their differences are minor: $M_w = 0.90M_L + 0.13$ (or $M_L = 0.97M_w + 0.38$) for shallow versus $M_w = 0.87M_L + 0.11$ (or $M_L = 1.03M_w + 0.40$) for deep. High-quality data for offshore deep events in the subduction zones are yet to be accumulated for better estimates of M_L–M_w relations; the structure dependency should be further investigated in future research.

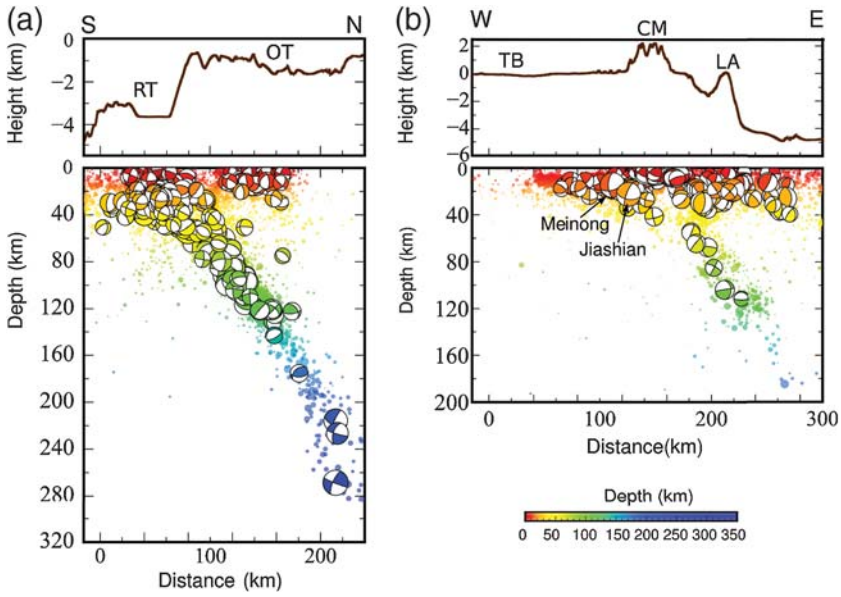


Figure 9. Cross sections of focal mechanisms overlapped with the background seismicity for profiles (a) AA′ and (b) BB′ indicated in Figure 1. The seismicity (circles) with $M_L \geq 2.5$ from CWB and all focal mechanisms (projected spheres) with $M_w \geq 4.0$ determined by our study are colored according to focal depth. The cross sections are plotted with one-to-one scale. Exaggerated topography is shown on the top of each profile. RT, Ryukyu trench; OT, Okinawa trough; TB, Tainan basin; CM, Central Mountain Range; LA, Luzon arc.

Seismotectonic Features Revealed by AutoBATS MTs

A complete well-constrained regional MT/CMT catalog is the key to understanding the relation of regional tectonic stress and strain (Kao and Jian, 2001; Zhu *et al.*, 2006; Hsu *et al.*, 2009; Martín *et al.*, 2015; Tseng *et al.*, 2016; Huang *et al.*, 2017). In Figure 9, we highlight two profiles with cross sections of the background seismicity from CWB and focal mechanisms determined from AutoBATS. The profile AA′ cuts through the Ryukyu subduction zone northeast of Taiwan (Fig. 1). The cross section clearly delineates the Wadati–Benioff Zone (WBZ) of the northward subducting Philippine Sea plate underneath the Eurasian plate, down to a depth of around 300 km (Fig. 9a). In the past, the focal mechanisms of intermediate-depth earthquakes near Taiwan have mostly been constrained from teleseismic studies for large events only (Kao, Shen, and Ma, 1998; Kao *et al.*, 2000). Based on regional data, our new AutoBATS MT catalog provides many solutions that are reasonably robust; the catalog has the potential to reveal details of features in the subduction zones (Fig. 9), although the sensitivity in focal depth is somewhat less than ideal due to the simple half-space model below Moho (Fig. 3). The cross section reveals that shallow normal-faulting events are dominant under the Okinawa trough north of the Ryukyu trench. It is remarkable to see the continuation of the focal mechanisms determined from shallow to intermediate-focus earthquakes, which can be used to understand the stress along the subducting slab.

Figure 9b shows another cross section in the northwest–southeast direction; the cross section passes through the Tainan basin, southern Central Mountain Range, southernmost Longitudinal Valley, and Luzon Arc on the Pacific Ocean. We can identify those mid-crust events (including the 2010 Jiashian and the 2016 Meinong M_w 6+ earthquakes) at a depth ~20 km near the Western Foothills of Taiwan. The focal mechanisms are consistent with former studies (Huang *et al.*, 2011; Lee *et al.*, 2016; Kanamori *et al.*, 2017). A cluster of normal-faulting events is also clearly observed at shallow depths (< 10 km) near the southern range of the Central Mountains. In the eastern end of the profile, the background seismicity depicts the subduction to a depth of ~200 km. Compared with the Ryukyu subduction zone in Figure 9a, the resolvable focal mechanisms here are far fewer; this is mainly because the earthquake activity is weaker. However, overall, the WBZ is clear, and the pattern of focal mechanisms is similar to the pattern found in the study of Kao *et al.* (2000). There seems to be another group of earthquakes near the eastern end of BB′ slightly dipping east under the Pacific to a depth of ~40 km in the mantle, which has not been observed before.

Conclusions

In this study, we presented a new automatic regional MT inversion algorithm, which we applied to determine over 3000 CMT solutions for seismic events that took place between May 1996 and April 2016 in the Taiwan area. The final focal mechanism of each earthquake was chosen from all the results with scanned settings including three station-selection groups, four velocity models, three frequency bands, and three isotropic component constrained strategies.

Both the focal mechanism and moment magnitude from AutoBATS show better consistency with Global CMT solutions than the current BATS catalog. Compared with the current BATS catalog, the AutoBATS also advances remarkably in the capability of resolving the focal mechanisms for earthquakes at a broader depth range (from 1 to 300 km). The fast and reliable AutoBATS inversion system is now implemented in the DMC of IES (DMC-IES). Once triggered by the CWB's earthquake alarm system, it only takes a short time (as short as 2 min) for the AutoBATS to publish an MT solution automatically on the Taiwan Earthquake Scientific Information System (Liang *et al.*, 2017) (TESIS; see Data and Resources). The DMC-IES also updates the final MT solutions monthly, with CWB providing the relocated earthquake catalog. The updated AutoBATS solutions will be online soon on the BATS website (see Data and Resources). The real-time triggered AutoBATS inversion algorithm, along with the earthquake alarm system from CWB, delivers fast and reliable basic earthquake information, including epicenter location, focal mechanism, and moment magnitude. The reliable AutoBATS MT catalog with relocated hypocenters can be used to improve our understanding of the seismotectonic background, seismic hazard, and regional stresses for the Taiwan area.

Data and Resources

The waveform data are provided by the Data Management Center of Broadband Array in Taiwan for Seismology (Institute of Earth Sciences, Academia Sinica, Taiwan, 1996) at http://bats.earth.sinica.edu.tw (last accessed October 2016). The relocated hypocenters were retrieved from the Geophysical Database Management System of Central Weather Bureau of Taiwan via http://gdms.cwb.gov.tw/index.php (last accessed October 2016). Moment tensor (MT) solutions of AutoBATS are available at the website of the Taiwan Earthquake Scientific Information System (http://tesis.earth.sinica.edu.tw). Software packages Seismic Analysis Code (SAC) and Generic Mapping Tools (GMT) were used for processing signals and plotting figures, respectively.

Acknowledgments

This work was supported by the Ministry of Science and Technology (Grant Numbers 105-2116-M-002-004, 105-2119-M-001-034, and 106-2116-M-002-008) and the Industrial Technology Research Institute of Taiwan. This work was significantly improved by the help of Wen-Hui Lee on proper operation of the real-time system for the AutoBATS moment tensors (MTs). The authors are grateful to the two anonymous reviewers for their constructive comments on the article.

References

Aki, K., and P. G. Richards (1980). *Quantitative Seismology: Theory and Methods*, W.H. Freeman, San Francisco, California.

Allen, R. V. (1978). Automatic earthquake recognition and timing from single traces, *Bull. Seismol. Soc. Am.* **68,** no. 5, 1521–1532.

Angelier, J., T.-Y. Chang, J.-C. Hu, C.-P. Chang, L. Siame, J.-C. Lee, B. Deffontaines, H.-T. Chu, and C.-Y. Lu (2009). Does extrusion occur at both tips of the Taiwan collision belt? Insights from active deformation studies in the Ilan Plain and Pingtung Plain regions, *Tectonophysics* **466,** nos. 3/4, 356–376, doi: 10.1016/j.tecto.2007.11.015.

Bernardi, F., J. Braunmiller, U. Kradolfer, and D. Giardini (2004). Automatic regional moment tensor inversion in the European–Mediterranean region, *Geophys. J. Int.* **157,** no. 2, 703–716, doi: 10.1111/j.1365-246x.2004.02215.x.

Bethmann, F., N. Deichmann, and P. M. Mai (2011). Scaling relations of local magnitude versus moment magnitude for sequences of similar earthquakes in Switzerland, *Bull. Seismol. Soc. Am.* **101,** no. 2, 515–534, doi: 10.1785/0120100179.

Bormann, P. (Editor) (2012). New manual of seismological observatory practice (NMSOP-2), in *IASPEI, GFZ German Research Centre for Geosciences, Potsdam*, doi: 10.2312/GFZ.NMSOP-2.

Braunmiller, J., U. Kradolfer, M. Baer, and D. Giardini (2002). Regional moment tensor determination in the European–Mediterranean area —Initial results, *Tectonophysics* **356,** nos. 1/3, 5–22, doi: 10.1016/s0040-1951(02)00374-8.

Cambaz, M. D., and A. K. Mutlu (2016). Regional moment tensor inversion for earthquakes in Turkey and its surroundings: 2008–2015, *Seismol. Res. Lett.* **87,** no. 5, 1082–1090, doi: 10.1785/0220150276.

Chen, K.-C., W.-T. Liang, Y.-H. Liu, W.-G. Huang, and J.-H. Wang (2008). Seismic moments of Taiwan's earthquakes evaluated from a regional broadband array, *Earth Planets Space* **60,** no. 6, 559–564, doi: 10.1186/bf03353118.

Chen, R.-Y., H. Kao, W.-T. Liang, T.-C. Shin, Y.-B. Tsai, and B.-S. Huang (2009). Three-dimensional patterns of seismic deformation in the Taiwan region with special implication from the 1999 Chi-Chi earthquake sequence, *Tectonophysics* **466,** nos. 3/4, 140–151, doi: 10.1016/j.tecto.2007.11.037.

Clinton, J. F., E. Hauksson, and K. Solanki (2006). An evaluation of the SCSN moment tensor solutions: Robustness of the M_w magnitude scale, style of faulting, and automation of the method, *Bull. Seismol. Soc. Am.* **96,** no. 5, 1689–1705, doi: 10.1785/0120050241.

Dahlen, F. A., and J. Tromp (1998). *Theoretical Global Seismology*, Princeton University Press, Princeton, New Jersey.

Deichmann, N. (2006). Local magnitude, a moment revisited, *Bull. Seismol. Soc. Am.* **96,** no. 4A, 1267–1277, doi: 10.1785/0120050115.

Dreger, D. S. (2003). TDMT_INV: Time domain seismic moment tensor inversion, in *International Handbook of Earthquake and Engineering Seismology*, H. Kanamori, P. C. Jennings, W. H. K. Lee, and C. Kisslinger (Editors), Vol. B, Academic Press, An Imprint of Elsevier Science, London, United Kingdom, 1627.

Dreger, D. S., and D. V. Helmberger (1993). Determination of source parameters at regional distances with three-component sparse network data, *J. Geophys. Res.* **98,** no. B5, 8107–8125, doi: 10.1029/93jb00023.

Dziewonski, A. M., T.-A. Chou, and J. H. Woodhouse (1981). Determination of earthquake source parameters from waveform data for studies of global and regional seismicity, *J. Geophys. Res.* **86,** no. B4, 2825–2852, doi: 10.1029/jb086ib04p02825.

Edwards, B., B. Allmann, D. Fäh, and J. Clinton (2010). Automatic computation of moment magnitudes for small earthquakes and the scaling of local to moment magnitude, *Geophys. J. Int.* **183,** no. 1, 407–420, doi: 10.1111/j.1365-246x.2010.04743.x.

Ekström, G., M. Nettles, and A. Dziewoski (2012). The global CMT project 2004–2010: Centroid-moment tensors for 13,017 earthquakes, *Phys. Earth Planet. In.* **200,** 1–9, doi: 10.1016/j.pepi.2012.04.002.

Frohlich, C. (2001). Display and quantitative assessment of distributions of earthquake focal mechanisms, *Geophys. J. Int.* **144,** no. 2, 300–308, doi: 10.1046/j.1365-246x.2001.00341.x.

Fukuyama, E., and D. S. Dreger (2000). Performance test of an automated moment tensor determination system for the future Tokai earthquake, *Earth Planets Space* **52,** no. 6, 383–392, doi: 10.1186/bf03352250.

Gasperini, P., B. Lolli, G. Vannucci, and E. Boschi (2012). A comparison of moment magnitude estimates for the European–Mediterranean and Italian regions, *Geophys. J. Int.* **190,** no. 3, 1733–1745, doi: 10.1111/j.1365-246X.2012.05575.x.

Hanks, T. C., and D. M. Boore (1984). Moment-magnitude relations in theory and practice, *J. Geophys. Res.* **89,** no. B7, 6229–6235, doi: 10.1029/jb089ib07p06229.

Hsu, Y.-J., S.-B. Yu, M. Simons, L.-C. Kuo, and H.-Y. Chen (2009). Interseismic crustal deformation in the Taiwan plate boundary zone revealed by GPS observations, seismicity, and earthquake focal mechanisms, *Tectonophysics* **479,** nos. 1/2, 4–18, doi: 10.1016/j.tecto.2008.11.016.

Huang, B.-H, Y.-L. Huang, S.-J. Lee, Y.-G. Chen, and J.-S. Jiang (2008). Initial rupture and processes of the Pingtung earthquake from near source strong-motion and records, *Terr. Atmos. Ocean. Sci.* **19,** no. 6, 547–554, doi: 10.3319/TAO.2008.19.6.547(PT).

Huang, G. D., S. W. Roecker, V. Levin, H. Wang, and Z. Li (2017). Dynamics of intra-continental convergence between the western Tarim basin and central Tien Shan constrained by centroid moment tensors of regional earthquakes, *Geophys. J. Int.* **208,** 561–576, doi: 10.1093/gji/ggw415.

Huang, H.-H., Y.-M. Wu, T.-L. Lin, W.-A. Chao, J. B. H. Shyu, C.-H. Chan, and C.-H. Chang (2011). The preliminary study of the 4 March 2010 M_w 6.3 Jiasian and Taiwan and earthquake sequence, *Terr. Atmos. Ocean. Sci.* **22,** no. 3, 283–290, doi: 10.3319/TAO.2010.12.13.01(T).

Huang, H.-H., Y.-M. Wu, X. Song, C.-H. Chang, S.-J. Lee, T.-M. Chang, and H.-H. Hsieh (2014). Joint V_P and V_S tomography of Taiwan: Implications for subduction-collision orogen, *Earth Planet. Sci. Lett.* **392,** 177–191, doi: 10.1016/j.epsl.2014.02.026.

Huang, W.-G., J.-H. Wang, B.-S. Huang, K.-C. Chen, T.-M. Chang, R.-D. Hwang, H.-C. Chiu, and C.-C. P. Tsai (2001). Estimates of source parameters for the 1999 Chi-Chi, Taiwan, earthquake based on Brune's source model, *Bull. Seismol. Soc. Am.* **91,** no. 5, 1190–1198.

Institute of Earth Sciences, Academia Sinica, Taiwan (1996). Broadband array in Taiwan for seismology, Institute of Earth Sciences, Academia Sinica, Taiwan, Other/Seismic Network, doi: 10.7914/SN/TW.

Ito, Y., S. Sekiguchi, T. Okada, R. Honda, K. Obara, and S. Hori (2006). Performance of regional distance centroid moment tensor inversion applied to the 2004 mid-Niigata prefecture earthquake, Japan, *Geophys. J. Int.* **167,** no. 3, 1317–1331, doi: 10.1111/j.1365-246x.2006.03109.x.

Jost, M. L., and R. Herrmann (1989). A student's guide to and review of moment tensors, *Seismol. Res. Lett.* **60,** no. 2, 37–57.

Kagan, Y. Y. (2002). Modern California earthquake catalogs and their comparison, *Seismol. Res. Lett.* **73,** no. 6, 921–929, doi: 10.1785/gssrl.73.6.921.

Kagan, Y. Y. (2003). Accuracy of modern global earthquake catalogs, *Phys. Earth Planet. In.* **135,** no. 2, 173–209, doi: 10.1016/s0031-9201(02)00214-5.

Kanamori, H., L. Ye, B.-S. Huang, H.-H. Huang, S.-J. Lee, W.-T. Liang, Y.-Y. Lin, K.-F. Ma, Y.-M. Wu, and T.-Y. Yeh (2017). A strong-motion hot spot of the 2016 Meinong, Taiwan, earthquake ($M_w = 6.4$), *Terr. Atmos. Ocean. Sci.* **28,** no. 5, 637–650, doi: 10.3319/TAO.2016.10.07.01.

Kao, H., and W.-P. Chen (2000). The Chi-Chi earthquake sequence: Active, out-of-sequence thrust faulting in Taiwan, *Science* **288,** no. 5475, 2346–2349.

Kao, H., and P.-R. Jian (1999). Source parameters of regional earthquakes in Taiwan: July 1995-December 1996, *Terr. Atmos. Ocean. Sci.* **10,** 585–604.

Kao, H., and P.-R. Jian (2001). Seismogenic patterns in the Taiwan region: insights from source parameter inversion of BATS data, *Tectonophysics* **333,** no. 1, 179–198, doi: 10.1016/s0040-1951(00)00274-2.

Kao, H., G.-C. Huang, and C.-S. Liu (2000). Transition from oblique subduction to collision in the northern Luzon arc-Taiwan region: Constraints from bathymetry and seismic observations, *J. Geophys. Res.* **105,** no. B2, 3059–3079, doi: 10.1029/1999jb900357.

Kao, H., P.-R. Jian, K.-F. Ma, B.-S. Huang, and C.-C. Liu (1998). Moment-tensor inversion for offshore earthquakes east of Taiwan and their implications to regional collision, *Geophys. Res. Lett.* **25,** no. 19, 3619–3622, doi: 10.1029/98GL02803.

Kao, H., Y.-H. Liu, and P.-R. Jian (2001). Source parameters of regional earthquakes in Taiwan: January-December, 1997, *Terr. Atmos. Ocean. Sci.* **12,** no. 2, 431–439, doi: 10.3319/TAO.2001.12.2.431(T).

Kao, H., Y.-H. Liu, W.-T. Liang, and W.-P. Chen (2002). Source parameters of regional earthquakes in Taiwan: 1999-2000 including the Chi-Chi earthquake sequence, *Terr. Atmos. Ocean. Sci.* **13,** no. 3, 279–298, doi: 10.3319/tao.2002.13.3.279(cce).

Kao, H., S. J. Shen, and K.-F. Ma (1998). Transition from oblique subduction to collision: Earthquakes in the southernmost Ryukyu arc-Taiwan region, *J. Geophys. Res.* **103,** no. B4, 7211–7229, doi: 10.1029/97JB03510.

Kubo, A., E. Fukuyama, H. Kawai, and K. Nonomura (2002). NIED seismic moment tensor catalogue for regional earthquakes around Japan: Quality test and application, *Tectonophysics* **356,** no. 1, 23–48, doi: 10.1016/s0040-1951(02)00375-x.

Kuo-Chen, H., F. T. Wu, and S. W. Roecker (2012). Three-dimensional *P* velocity structures of the lithosphere beneath Taiwan from the analysis of TAIGER and related seismic data sets, *J. Geophys. Res.* **117,** no. B6, doi: 10.1029/2011JB009108.

Lallemand, S., Y. Font, H. Bijwaard, and H. Kao (2001). New insights on 3-D plates interaction near Taiwan from tomography and tectonic implications, *Tectonophysics* **335,** no. 3, 229–253, doi: 10.1016/S0040-1951(01)00071-3.

Lee, E.-J., P. Chen, T. H. Jordan, and L. Wang (2011). Rapid full-wave centroid moment tensor (CMT) inversion in a three-dimensional earth structure model for earthquakes in southern California, *Geophys. J. Int.* **186,** no. 1, 311–330, doi: 10.1111/j.1365-246X.2011.05031.x.

Lee, S.-J., W.-T. Liang, H.-W. Cheng, F.-S. Tu, K.-F. Ma, H. Tsuruoka, H. Kawakatsu, B.-S. Huang, and C.-C. Liu (2014). Towards real-time regional earthquake simulation I: Real-time moment tensor monitoring (RMT) for regional events in Taiwan, *Geophys. J. Int.* **196,** no. 1, 432–446, doi: 10.1093/gji/ggt371.

Lee, S.-J., W.-T. Liang, and B.-S. Huang (2008). Source mechanisms and rupture processes of the 26 December 2006 Pingtung earthquake doublet as determined from the regional seismic records, *Terr. Atmos. Ocean. Sci.* **19,** no. 6, 555–565, doi: 10.3319/TAO.2008.19.6.555(PT).

Lee, S.-J., T.-Y. Yeh, and Y.-Y. Lin (2016). Anomalously large ground motion in the 2016 ML 6.6 Meinong, Taiwan, earthquake: A synergy effect of source rupture and site amplification, *Seismol. Res. Lett.* **87,** no. 6, 1319–1326, doi: 10.1785/0220160082.

Liang, W.-T., J.-C. Lee, K. H. Chen, and N.-C. Hsiao (2017). Citizen earthquake science in Taiwan: From science to hazard mitigation, *J. Disaster Res.* **12,** no. 6, 1174–1181, doi: 10.20965/jdr.2017.p1174.

Liang, W.-T., Y.-H. Liu, and H. Kao (2004). Source parameters of regional earthquakes in Taiwan: January-December, 2002, *Terr. Atmos. Ocean. Sci.* **15,** 727–742, doi: 10.3319/TAO.2004.15.4.727(T).

Lin, J.-Y., J.-C. Sibuet, C.-S. Lee, S.-K. Hsu, and F. Klingelhoefer (2007). Origin of the southern Okinawa Trough volcanism from detailed seismic tomography, *J. Geophys. Res.* **112,** no. B8, doi: 10.1029/2006jb004703.

Martín, R., D. Stich, J. Morales, and F. Mancilla (2015). Moment tensor solutions for the Iberian-Maghreb region during the IberArray deployment (2009–2013), *Tectonophysics* **663,** 261–274, doi: 10.1016/j.tecto.2015.08.012.

Mellman, G., L. Burdick, and D. Helmberger (1975). Determination of source parameters from body wave seismograms, *Earthquake Notes* **46,** no. 1, 44.

Nakano, M., H. Kumagai, and H. Inoue (2008). Waveform inversion in the frequency domain for the simultaneous determination of earthquake source mechanism and moment function, *Geophys. J. Int.* **173,** no. 3, 1000–1011, doi: 10.1111/j.1365-246x.2008.03783.x.

Pondrelli, S., A. Morelli, G. Ekström, S. Mazza, E. Boschi, and A. Dziewonski (2002). European–Mediterranean regional centroid-moment tensors: 1997–2000, *Phys. Earth Planet. In.* **130,** no. 1, 71–101, doi: 10.1016/s0031-9201(01)00312-0.

Rau, R.-J., and F. T. Wu (1995). Tomographic imaging of lithospheric structures under Taiwan, *Earth Planet. Sci. Lett.* **133,** no. 3, 517–532, doi: 10.1016/0012-821x(95)00076-o.

Ristau, J. (2008). Implementation of routine regional moment tensor analysis in New Zealand, *Seismol. Res. Lett.* **79,** no. 3, 400–415, doi: 10.1785/gssrl.79.3.400.

Ristau, J. (2009). Comparison of magnitude estimates for New Zealand earthquakes: Moment magnitude, local magnitude, and teleseismic

body-wave magnitude, *Bull. Seismol. Soc. Am.* **99,** no. 3, 1841–1852, doi: 10.1785/0120080237.

Ristau, J., G. C. Rogers, and J. F. Cassidy (2003). Moment magnitude-local magnitude calibration for earthquakes off Canada's west coast, *Bull. Seismol. Soc. Am.* **93,** no. 5, 2296–2300, doi: 10.1785/0120030035.

Rueda, J., and J. Mezcua (2005). Near-real-time seismic moment-tensor determination in Spain, *Seismol. Res. Lett.* **76,** no. 4, 455–465, doi: 10.1785/gssrl.76.4.455.

Scognamiglio, L., E. Tinti, and A. Michelini (2009). Real-time determination of seismic moment tensor for the Italian region, *Bull. Seismol. Soc. Am.* **99,** no. 4, 2223–2242, doi: 10.1785/0120080104.

Shin, T.-C. (1993). The calculation of local magnitude from the simulated Wood-Anderson seismograms of the short-period seismograms in the Taiwan area, *Terr. Atmos. Ocean. Sci.* **4,** 155–170, doi: 10.3319/TAO.1993.4.2.155(T).

Sileny, J., P. Campus, and G. F. Panza (1996). Seismic moment tensor resolution by waveform inversion of a few and local noisy records —I. Synthetic and tests, *Geophys. J. Int.* **126,** 605–619.

Sipkin, S. A. (1986). Estimation of earthquake source parameters by the inversion of waveform data: Global seismicity, 1981–1983, *Bull. Seismol. Soc. Am.* **76,** no. 6, 1515–1541.

Stich, D., C. J. Ammon, and J. Morales (2003). Moment tensor solutions for small and moderate earthquakes in the Ibero-Maghreb region, *J. Geophys. Res.* **108,** no. B3, doi: 10.1029/2002jb002057.

Stump, B. W., and L. R. Johnson (1977). The determination of source properties by the linear inversion of seismograms, *Bull. Seismol. Soc. Am.* **67,** no. 6, 1489–1502.

Tange, O. (2011). GNU Parallel—The command-line power tool, *login: The USENIX Magazine* **36,** no. 1, 42–47, doi: 10.5281/zenodo.16303.

Tseng, T.-L., H.-C. Hsu, P.-R. Jian, B.-S. Huang, J.-C. Hu, and S.-L. Chung (2016). Focal mechanisms and stress variations in the Caucasus and northeast Turkey from constraints of regional waveforms, *Tectonophysics* **691,** 362–374, doi: 10.1016/j.tecto.2016.10.028.

Vallée, M., J. Charléty, A. M. Ferreira, B. Delouis, and J. Vergoz (2011). SCARDEC: A new technique for the rapid determination of seismic moment magnitude, focal mechanism and source time functions for large earthquakes using body-wave deconvolution, *Geophys. J. Int.* **184,** no. 1, 338–358, doi: 10.1111/j.1365-246x.2010.04836.x.

Wallace, T. C., D. V. Helmberger, and G. R. Mellman (1981). A technique for the inversion of regional data in source parameter studies, *J. Geophys. Res.* **86,** no. B3, 1679, doi: 10.1029/jb086ib03p01679.

Wang, H.-L., L. Zhu, and H.-W. Chen (2010). Moho depth variation in Taiwan from teleseismic receiver functions, *J. Asian Earth Sci.* **37,** no. 3, 286–291, doi: 10.1016/j.jseaes.2009.08.015.

Yao, Z., and D. Harkrider (1983). A generalized reflection-transmission coefficient matrix and discrete wavenumber method for synthetic seismograms, *Bull. Seismol. Soc. Am.* **73,** no. 6A, 1685–1699.

Yen, Y.-T., and K.-F. Ma (2011). Source-scaling relationship for M 4.6–8.9 earthquakes, specifically for earthquakes in the collision zone of Taiwan, *Bull. Seismol. Soc. Am.* **101,** no. 2, 464–481, doi: 10.1785/0120100046.

Zhu, L., and D. V. Helmberger (1996). Advancement in source estimation techniques using broadband regional seismograms, *Bull. Seismol. Soc. Am.* **86,** no. 5, 1634–1641.

Zhu, L., and L. A. Rivera (2002). A note on the dynamic and static displacements from a point source and in multilayered media, *Geophys. J. Int.* **148,** 619–627, doi: 10.1046/j.1365-246x.2002.01610.x.

Zhu, L., N. Akyol, B. J. Mitchell, and H. Sozbilir (2006). Seismotectonics of western Turkey from high resolution earthquake relocations and moment tensor determinations, *Geophys. Res. Lett.* **33,** no. 7, doi: 10.1029/2006gl025842.

Department of Geosciences
National Taiwan University
No. 1, Section 4, Roosevelt Road
Taipei 10617, Taiwan
d01224005@ntu.edu.tw
tailintseng@ntu.edu.tw
(P.-R.J., T.-L.T.)

Institute of Earth Sciences
Academia Sinica
No. 128, Section 2, Academia Road
Taipei 11529, Taiwan
wtl@earth.sinica.edu.tw
(W.-T.L.)

Institute of Earth Sciences
National Taiwan Ocean University
No. 2, Beining Road
Keelung 20224, Taiwan
eric791130@gmail.com
(P.-H.H.)

Manuscript received 16 August 2017;
Published Online 13 February 2018

View publication stats